AIAA SciTech Forum
8–12 January 2018, Kissimmee, Florida
2018 AIAA Atmospheric Flight Mechanics Conference

10.2514/6.2018-0295

Online Near Real-Time System Identification on a Fixed-Wing Small Unmanned Air Vehicle

Han-Hsun Lu,* Cameron T. Rogers,* Vinicius G. Goecks ,* and John Valasek†
Texas A&M University, College Station, TX, 77843–3141, USA

An online near real-time system identification system is developed for the onboard generation of locally linear models of Small Unmanned Air Systems. Angle-of-attack and sideslip angle are measured rather than estimated, and automated control surface excitation inputs consisting of doublets, triplets, and frequency sweeps are implemented and used to assure consistency in the excitation and to eliminate errors introduced by manually applied user inputs. A real-time vehicle monitoring system is used to provide a human-in-the-loop model update capability, with a goal of ensuring the safety of the vehicle. A combined lateral/directional and longitudinal excitation is developed and demonstrated for identifying a full dynamic system and representing it in state-space form. The methodology is demonstrated with flight tests of a fixed-wing Small Unmanned Air System, with locally linear models generated onboard the vehicle during flight. Results presented in the paper show that the system is capable of reliably and repeatedly generating accurate locally linear models that are suitable for real-time flight control design using model based control techniques and post-flight modal analysis.

Nomenclature

$\boldsymbol{x}$	State vector	B_{m}	Modal input matrix
$\boldsymbol{y}$	Measurement vector	C_{m}	Modal output matrix
$\bar{A}$	Augmented observer system matrix	ζ	Damping ratio
$\bar{B}$	Augmented observer input matrix	α	Angle-of-attack, deg
$\boldsymbol{v}$	Stacked input and output vector	β	Sideslip angle, deg
G	Arbitrary matrix	$\phi,\ \theta$	Euler Attitude Angles
$\bar{\boldsymbol{y}}$	Augmented measurement vector	δ_a	Aileron deflection, deg
$\bar{Y}$	Observer Markov Parameters (OMP)	δ_r	Rudder deflection, deg
$\bar{V}$	Stacked input and output matrix	δ_T	Throttle command, RPM
p	Number of time shifts in the Hankel matrices	δ_e	Elevator deflection, deg
H	Hankel matrix	*Subscript*	
$\hat{A}$	Identified system matrix	o	First instance
$\hat{B}$	Identified input matrix	k	Instance number
$\hat{C}$	Identified output matrix		
$\hat{D}$	Identified carry-through matrix		

*Graduate Research Assistant, Vehicle Systems & Control Laboratory, Aerospace Engineering Department, Student Member AIAA. {hanhsun.lu,crogers,vinicius.goecks}@tamu.edu
†Professor and Director, Vehicle Systems & Control Laboratory, Aerospace Engineering Department, Fellow AIAA. valasek@tamu.edu

I. Introduction

Flight control synthesis for aircraft with large flight envelopes and wide ranges of angle-of-attack and sideslip angle require much ground based and flight based testing in order to generate accurate locally linear models. The traditional aircraft modeling process usually uses first-order Data Compendium (DATCOM) methods accompanied with low order Computational Fluid Dynamics (CFD)/high order CFD. Wind tunnel testing is then conducted for determining aerodynamic coefficients and stability and control derivatives. However, the high cost of wind tunnel testing restricts the number of experimental tests that can be conducted.[1] Finally, flight tests are performed for validation and verification of the model. Iterations to this process are applied as necessary, and model development and refinement is a continual process that requires more iterations when flight control design is being conducted. The accumulated cost for human resources, test facilities, and test materials over several years can require a large group of experts with abundant funding and schedule.

After analytical/computational modeling and wind tunnel testing, system identification flight testing of aircraft requires precise piloted maneuvers that are ideally flown in low wind or dead calm environmental conditions. Inaccurate models are often generated for SUAS due to the inability to capture the errors induced by the pilot or environment during the flight. Additionally, conventional post flight data analysis processes require more flights, resulting in increased development costs. In the case of agile development the process described above can impact the ability to conduct rapid prototyping and rapid modeling. Figure 1 illustrates how online, near real-time system identification can be used for rapid SUAS development.

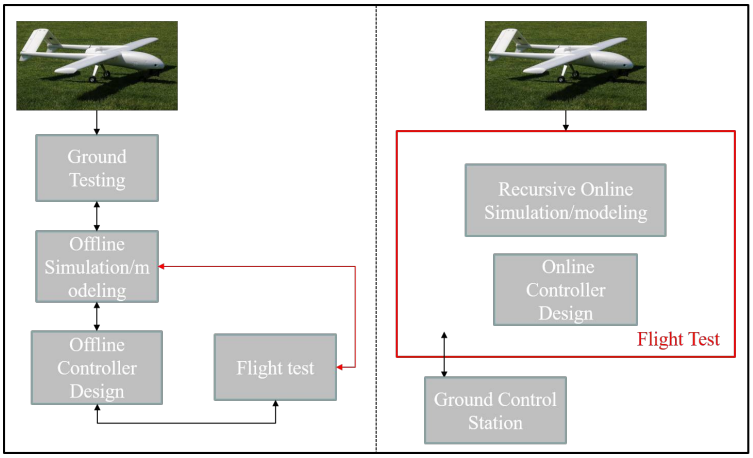

Figure 1: Comparison of proposed online system identification methodology with conventional flight system modeling process.

Online near real-time system identification updates the system model on-the-fly and can be used for vehicles with time varying dynamics. Several real-time system identification studies have been conducted in the past ten years at different research organizations,[2,3] applying methods either under the broad recursive least squares parameter estimation category or frequency domain analysis category. For nonlinear systems the Artificial Neural Network (ANN) has shown to be a promising candidate for nonlinear system identification. Models with a two-layer neural network and radial basis functions have been applied for nonlinear aircraft dynamics.[4] However, when the number of nodes and system output dimensions increase the performance tends to decrease drastically due to the system complexity. Since 2014 NASA Langley Research Center (LaRC) has been conducting research in global aerodynamic modeling for aircraft.[5] This method is based on the System IDendtification Programs for AirCraft (SIDPAC)[6] along with reinforcement learning to perform effective estimation of the non-dimensional aerodynamic force and moment coefficients. The method has also been shown to provide accurate models for manned aircraft.[7] Applying this method to SUAS for aerodynamic modeling requires precise measurements or estimates of the inertias of the system. With limited payload capacity and onboard computational resources, the capability to generate high-fidelity flight models that can be applied globally is restricted.

Observer Kalman-filter IDentification (OKID) is a linear identification method often used in the aerospace community. The method does not require vehicle specific knowledge of the system being modeled, and therefore is a good candidate for online near real-time system identification for vehicles with time varying

characteristics. Valasek and Chen[8] demonstrated in nonlinear, non-real time simulation that OKID is feasible for on demand, online system identification of fixed-wing aircraft longitudinal and lateral/direction models. OKID has also been demonstrated to provide good offline results for Small Unmanned Aircraft Systems (SUAS).[9,10] This paper extends the work of[10] by developing and demonstrating an online system identification capability with real-time ground-to-air data transfer, high frequency data acquisition, and near real-time onboard identification of locally-linear models during flight.

The paper is organized as follows. Section II introduces the airframe and flight test instrumentation, including the sensors, data acquisition system, and communication system. Section III details the OKID algorithm used for generating discrete linear state space models. The methods used for online near real-time identification including automated excitation, mode selection and the online system identification methods are detailed in Section IV. Section V presents the flight test results and Section VI presents conclusions and recommendations for extending this work.

II. Flight Test Instrumentation

The flight test instrumentation consists of a data acquisition system and the Clark multi-agent control framework. The system provides high frequency data measurements of all aircraft states and control surface deflections while maintaining real-time air-to-ground data communication.

II.A. Developmental Flight Test Instrumentation

The Developmental Flight Test Instrumentation (DFTI)[11] is a modular data acquisition system that records system states and control effector positions at 100 Hz in a compact form factor for easy porting between different SUAS. The modular software is designed to support multiple sensors and airframes while interfacing with other systems through IP communications. DFTI is implemented as a Linux command line application in C++11 using the Qt5 framework to allow for easy concurrency and threading with the signal/slot paradigm.

Figure 2: Developmental flight test instrumentation hardware.

The hardware architecture and its connection subsystems is shown in Fig. 3. The capability of measuring all flight critical states minimizes the probability of estimation error due to approximations. A VectorNav VN-200 is used as the Inertial Measurement Unit (IMU) providing attitude angles, angular rates, and GPS position. The Aeroprobe five-hole probe along with the µADCair data computer measures velocity, angle-of-attack, and sideslip angle. The Beaglebone Black Rev C is selected as the micro processor for data acquisition and data parsing due to the number of universal asynchronous receiver-transmitter ports. All states are collected at 100 Hz with a 5 Hz GPS signal.

Previous instrumentation used by the authors recorded commanded surface positions as pulse width

modulated signals.[9,10] The drawbacks of this approach are identifying the effect of the actuator dynamics as part of the aircraft dynamics, and the inability to detect failures in the actuator. To directly measure control surface deflection angles the current system uses seven BI Technologies 6127V1A360L.5FS linear potentiometers which are rigidly mounted to the airframe and connected to the control surfaces by standard RC control horns and rods. An Arduino UNO is used to acquire analog measurements of the control surfaces directly. Specifications of the individual sensors and processors can be found in Table 1.

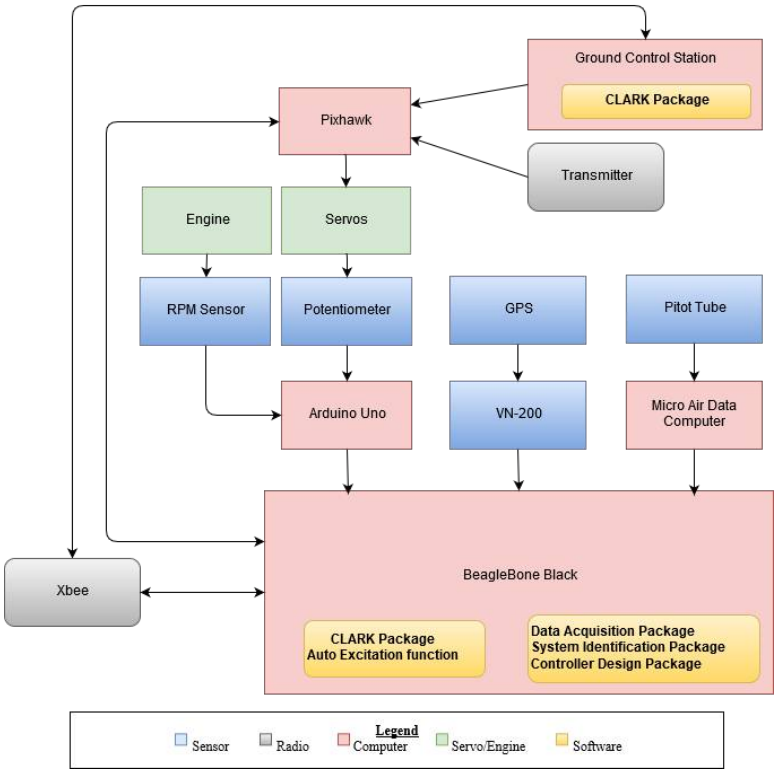

Figure 3: Hardware Architecture and Sub-System Components.

II.B. Clark

Clark[12] is a multi-agent control framework that provides a user with the ability to autonomously command various inputs from a mission control station. It is executed as a separate command line application on the BeagleBone Black as shown in Fig. 3. The framework consists of a three-tiered software architecture connecting the autopilot, radio transceiver, and connected payloads. An abstraction layer provides a specific location for implementing control. No payloads are connected for the work presented in this paper. Fig. 4 depicts this three-tier architecture.

The aircraft is not required to land to switch testing parameters during flight since all changes can be made on-the-fly with Clark. Clark provides a means for precisely generating doublets, 3-2-1-1's, and sine sweeps of varying amplitudes, periods, and frequency as system identification inputs from a ground console. These automated inputs are generated by a predefined mission algorithm contained in the Clark mission class and then commanded using the autopilot interface class. The autopilot interface utilizes MAVLink, a common small air vehicle protocol, to communicate with the autopilot. The mission algorithm receives input over an XBee Pro 900HP network at a rate of 5 Hz. It is over this network that parameters are sent from the ground to the vehicle. The excitation inputs are triggered by the pilot through an auxiliary channel on the remote control transmitter.

II.C. Flight Vehicle

The 1/4 scale Hangar-9 PA-18 Super Cub SUAS is the base air vehicle used for testing the flight test instrumentation system. The $700 commercial off-the-shelf (COTS) Super Cub has a wingspan of 8.8 feet,

Table 1: DFTI Specifications

Avionics	
Instrumentation Computer	BeagleBone Black Rev. C
Processor	TI AM335x Sitara 1 GHz ARM® Cortex A-8
RAM	512 MB DDR3
Air Data System	
Air Data Computer	Aeroprobe Corporation Micro Air Data Computer µADC
Flow Angle Range	±20°
Airspeed Resolution	$0.36\,\mathrm{m\,s^{-1}}$
Max Flow Angle Error	±1.0°
Max Calibrated Airspeed	$64\,\mathrm{m\,s^{-1}}$
Current Draw	<390 mA @ 12 V DC
Inertial Navigation System	
INS	VectorNav VN-200
Accuracy (Pitch/Roll)	0.5 °RMS
Accuracy (Heading)	0.5 °RMS
Angular Resolution	<0.05°
Gyro Noise Density	$0.0035\,^\circ\,\mathrm{s^{-1}}\,\sqrt{\mathrm{Hz}}$
Gyro Alignment Error	±0.05°
Gyro Resolution	<0.02°

empty weight of 16.6 pounds, and endurance of 30-45 minutes with extended batteries. The aircraft has a 295 kV E-Flite Power 110 electric brushless motor, 85 A HV brushless Electronic Speed Controller (ESC), and an APC 19×10E propeller. Due to its rugged construction, short takeoff and landing performance, and excellent low speed flying qualities it is suitable for rough field operations. The Super Cub also excels at carrying multiple sensor payloads. Figure 5 shows the Super Cub vehicle used for testing.

III. Observer/Kalman Filter Identification

During the 1980's many system identification methods have been developed to identify linear state-space model for spacecraft and aircraft with flexible structural characteristics. The majority of these methods are based on Fast Fourier Transform (FFT), Maximum Likelihood Estimation, and least squares.[13] A drawback of the FFT and MLE methods is that a somewhat rich input is required to prevent ill-conditioned computation. Developed in the 1990's by Juang,[14] the Observer/Kalman Filter Identification algorithm (OKID) method is a direct Kalman filter gain approach. OKID is formulated in time-domain and is capable of handling general response data. This is especially valuable for aircraft modeling since pure impulse excitations are difficult to apply and noise/ signal ratio of sensing data are usually high. It also has the benefits of allowing for nonzero initial conditions and does not require the response to decay to steady-state before enough data is collected to process. The present work is an extension of the concept that OKID can be successfully used to identify state-space models of flight vehicles. OKID has the benefit of only requiring input/output time histories to perform system identification. This reduces the amount of a priori system specific information required to perform system identification. Therefore, OKID is chosen as the method for system identification in the present work.

The basic formulation of the OKID algorithm begins with the linearized, discrete-time, state-space equations augmented with an observer gain:

$$\begin{aligned} \boldsymbol{x}(k+1) &= \bar{A}\boldsymbol{x}(k) + \bar{B}\boldsymbol{v}(k)\,, \\ \boldsymbol{y}(k) &= C\boldsymbol{x}(k) + D\boldsymbol{u}(k) \end{aligned} \tag{1}$$

where $\boldsymbol{x}(k) \in \mathbb{R}^n$, $\boldsymbol{y}(k) \in \mathbb{R}^m$, $\boldsymbol{u}(k) \in \mathbb{R}^r$, are state, output and control inputs with dimension of n, m, and

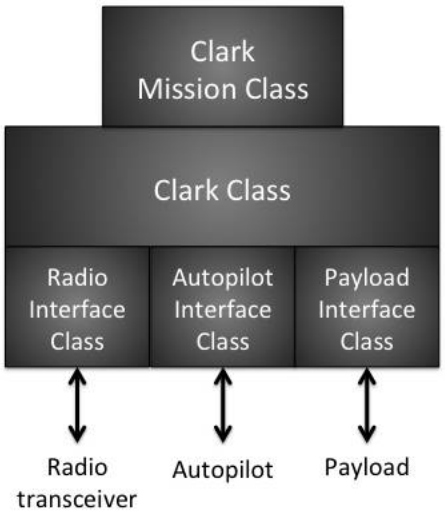

Figure 4: Three tier architecture of the Clark framework.

r respectively with

$$\begin{aligned} \bar{A} &= A + GC\,, \\ \bar{B} &= [B + GD, -G]\,, \\ \boldsymbol{v}(k) &= \begin{bmatrix} \boldsymbol{u}(k) \\ \boldsymbol{y}(k) \end{bmatrix}\,. \end{aligned} \tag{2}$$

and $G \in \mathbb{R}^{n\times m}$ is an arbitrary matrix chosen to make the matrix $\bar{A}$ stable. Assuming zero initial conditions, $\boldsymbol{x} = 0$ and integer p satisfying $CA^kB \approx 0$ for $k \geq p$. By substituting and iterating through each time step using Eq. (1), the Observer Markov Parameters (OMP) which are functions of an input-output relationship become

$$\bar{\boldsymbol{y}} = C\bar{A}^p\boldsymbol{x} + \bar{Y}\bar{V} \tag{3}$$

where

$$\begin{aligned} \bar{y} &= \begin{bmatrix} \boldsymbol{y}(p) & \boldsymbol{y}(p+1) & \cdots & \boldsymbol{y}(l-1) \end{bmatrix}\,, \\ \bar{Y} &= \begin{bmatrix} D & C\bar{B} & C\bar{A}\bar{B} & \cdots & C\bar{A}^{(p-1)}\bar{B} \end{bmatrix}\,, \\ \bar{V} &= \begin{bmatrix} \boldsymbol{u}(p) & \boldsymbol{u}(p+1) & \cdots & \boldsymbol{u}(l-1) \\ \boldsymbol{v}(p-1) & \boldsymbol{v}(p) & \cdots & \boldsymbol{v}(l-2) \\ \boldsymbol{v}(p-2) & \boldsymbol{v}(p-1) & \cdots & \boldsymbol{v}(l-3) \\ \vdots & \ddots & \cdots & \vdots \\ \boldsymbol{v}(0) & \boldsymbol{v}(1) & \cdots & \boldsymbol{v}(l-p-1) \end{bmatrix}\,. \end{aligned} \tag{4}$$

The matrix $\bar{Y}$ is partitioned such that

$$\bar{Y} = \begin{bmatrix} D & C\bar{B} & C\bar{A}\bar{B} & \cdots & C\bar{A}^{(p-1)}\bar{B} \end{bmatrix} = \begin{bmatrix} Y_0 & Y_1 & Y_2 & \cdots & Y_p \end{bmatrix} \tag{5}$$

Figure 5: Hangar-9 1/4-Scale PA-18 Super Cub

from which the OMP are obtained:

$$\begin{aligned}
\bar{Y}_0 &= D\,, \\
\bar{Y}_k &= C\bar{A}^{(k-1)}\bar{B} \\
&= \begin{bmatrix} C(A+GC)^{(k-1)}(B+GD) & -C(A+GC)^{(k-1)}G \end{bmatrix} \\
&= \begin{bmatrix} \bar{Y}_k^{(1)} & -\bar{Y}_k^{(2)} \end{bmatrix} \quad k = 1, 2, 3, \ldots\,.
\end{aligned} \tag{6}$$

The general relationship between the actual System Markov Parameters and the OMP can be shown to be:

$$\begin{aligned}
D &= Y_0 = \bar{Y}_0\,, \\
Y_k &= Y_k^{(1)} - \sum_{i=1}^{k} \bar{Y}_i^{(2)} Y_{(k-i)} \quad \text{for } k = 1, \ldots, p\,, \\
Y_k &= -\sum_{i=1}^{p} \bar{Y}_i^{(2)} Y_{(k-i)} \quad \text{for } k = p+1, \ldots, \infty\,.
\end{aligned} \tag{7}$$

The next step is to use singular value decomposition (SVD) on the Hankel matrix.

$$\begin{aligned}
H(k-1) &= \begin{bmatrix} Y_k & Y_{k+1} & \cdots & Y_{k+\beta-1} \\ Y_{k+1} & Y_{k+2} & \cdots & Y_{k+\beta} \\ \vdots & \vdots & \ddots & \vdots \\ Y_{k+\alpha-1} & Y_{k+\alpha} & \cdots & Y_{k+\alpha+\beta-2} \end{bmatrix} \\
H(0) &= P_n \Sigma Q_n^{\mathsf{T}}\,.
\end{aligned} \tag{8}$$

The Eigensystem Realization Algorithm is then used to solve the Hankel matrix for the desired state-space realization (A, B, C, D):

$$\begin{aligned}
\hat{A} &= \Sigma_n^{-1/2} P_n^{\mathsf{T}} H(1) Q_n \Sigma_n^{-1/2}\,, \\
\hat{B} &= \Sigma_n^{1/2} Q_n^{\mathsf{T}}\,, \\
\hat{C} &= P_n \Sigma_n^{1/2}\,, \\
\hat{D} &= Y_0\,.
\end{aligned} \tag{9}$$

Note that $\hat{A}$, $\hat{B}$, and $\hat{C}$ are the estimated system matrices arrived at by the system identification using OKID. The $(\hat{A}, \hat{B}, \hat{C}, \hat{D})$ represent the identified discrete linear state-space system when used in Eq. (10).

$$\begin{aligned} \boldsymbol{x}(k+1) &= \hat{A}\boldsymbol{x}(k) + \hat{B}\boldsymbol{u}(k)\,, \\ \boldsymbol{y}(k) &= \hat{C}\boldsymbol{x}(k) + \hat{D}\boldsymbol{u}(k)\,. \end{aligned} \tag{10}$$

IV. Online System Identification

IV.A. Automated Excitation

Previous flight test results have shown that the consistency and quality of piloted excitation relies heavily on training and experience.[15] The need is for automated excitations to provide repeatable, efficient, and precise excitations for online system identification. A human-in-the-loop auto-excitation system was developed using the Clark communication system described in Section II.B, and supports a Graphical User Interface (GUI) for ease of interfacing between the Ground Control Station (GCS) and the air vehicle. The GCS operator assigns the excitation method, choice of servo to inject the input to a particular control effector, input amplitude, and excitation characteristics though the GUI shown in Fig. 6. Two approaches are applied for system identification input design. The first approach requires little to no *a priori* knowledge of the behavior of the dynamical system. Impulse excitation and frequency sweeps are in this category, where the goal is to excite all dynamic modes across a large frequency range. The second approach requires *a priori* understanding of the system and designs the input with respect to the dynamic modes.

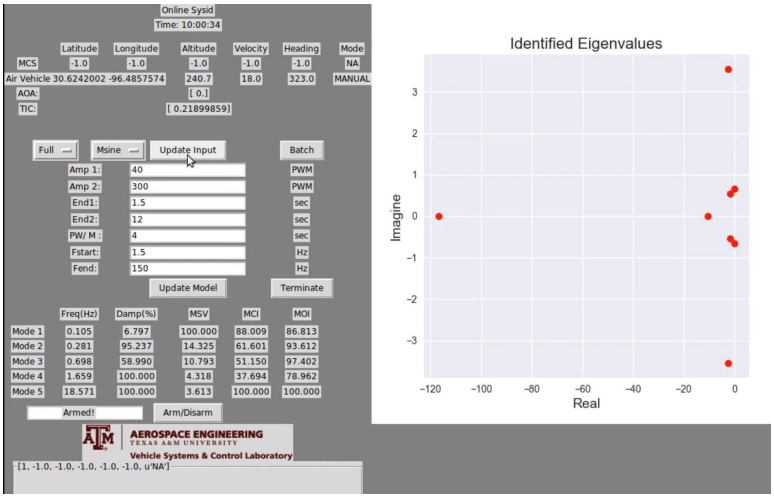

Figure 6: Ground-air communication GUI through Clarkview

To excite the rigid-body dynamic modes the maneuver time length, control surface magnitude, maneuver sequence, and input correlations are specified through Clark. Several flight test maneuvers have been discussed in [13,16,17] for the purpose of performing efficient excitation for system identification. Schroeder[18] has shown that by adjusting the phase angles of a periodic signal with a given power spectrum

$$u(t) = \sum_{k=1}^{M} A_k \cos\left(\frac{2\pi k\tau(t)}{T} + \phi_k\right), \quad t = 0, 1, \cdots, N-1 \tag{11}$$

the peak-to-peak amplitude can be minimized, where M is the number of harmonically related frequencies and ϕ_k are phase angles. By calculating the Relative Peak Factor (RPF) as in Eq. (12), the efficiency of the excitation can be quantified.

$$RPF(\boldsymbol{u}) = \frac{\frac{\max(\boldsymbol{u}) - \min(\boldsymbol{u})}{2}}{2\sqrt{2}\; rms(\boldsymbol{u})} = \frac{PF(\boldsymbol{u})}{\sqrt{2}} \tag{12}$$

Morelli[19] applied the multi-sinusoid sweep and showed that by carefully designing the input frequencies the multi-sine excitation method provides an efficient input signal that is suitable for multiple surface concurrent

excitation. Therefore, doublets, 3-2-1-1, sinusoid sweeps, and multi-sine sweeps are all implemented in the automated control function and are applied by Clark through the Pixhawk2 auxiliary ports.[20]

To reduce the risk of software and flight computer failure a hardware fail-safe multiplexer is connected to both the RC and auxiliary ports of the Pixhawk2. This provides the pilot with the ability to override any auto-excitation. The use of the failsafe multiplexer ensures that even if the software is stuck in a computational loop, the pilot can safely regain control of the vehicle immediately. The failsafe multiplexer and Pixhawk2 are shown in Fig. 7.

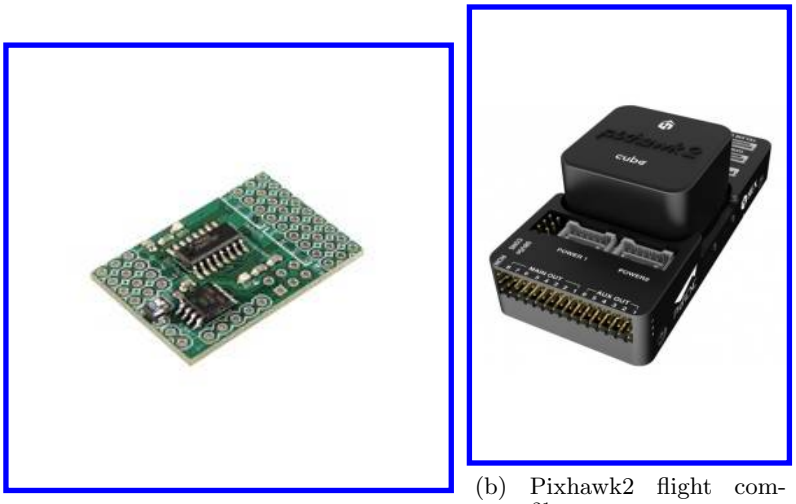

(a) Fail-safe multiplexer

(b) Pixhawk2 flight computer[21]

Figure 7: Hardware for auto-excitation

IV.B. Mode Selection

Mode Singular Values (MSV), Modal Controllability Index (MCI), and Modal Observability Index (MOI) are used for the selection of the identified modes.[22,23] The indicators are calculated online by

$$\begin{aligned} MCI &= 100 \cdot \ |B_{\mathrm{m}}| \max |B_{\mathrm{m}}| \\ MOI &= 100 \cdot \ |C_{\mathrm{m}}| \max |C_{\mathrm{m}}| \\ MSV &= 100 \cdot \frac{\frac{\sqrt{|B_{\mathrm{m}}| \cdot |C_{\mathrm{m}}|}}{|1-|\zeta||}}{\max \frac{\sqrt{|B_{\mathrm{m}}| \cdot |C_{\mathrm{m}}|}}{|1-|\zeta||}} \end{aligned} \tag{13}$$

where $B_{\mathrm{m}} \in \mathbb{R}^{nm \times r}$ is the modal input matrix, nm is the number of modes, $C_{\mathrm{m}} \in \mathbb{R}^{m \times nm}$ is the modal output matrix, and $\zeta \in \mathbb{R}^{nm}$ is the eigenvalue vector.

IV.C. Model Comparison

The user is provided with the capability to update the stored nominal model if desired. To make this decision it is important to have a quantified index. A simple but efficient method of comparing two different identified models is to analyze the difference between two generated signals. The Theil Inequality Coefficient (TIC) is a normalized metric that quantifies the identified response in terms of residuals. Summing the TIC for each output i using Eq. (14) yields a total TIC of the identified model. Dividing the total TIC value by the number of outputs m the averaged TIC value can be calculated.

$$\mathcal{T}_i = \frac{\sqrt{\frac{1}{N}\sum_{k=1}^{N}\left[\hat{y}_i(k) - y_i(k)\right]^2}}{\sqrt{\frac{1}{N}\sum_{k=1}^{N}\left[\hat{y}_i(k)\right]^2} + \sqrt{\frac{1}{N}\sum_{k=1}^{N}\left[y_i(k)\right]^2}} \quad i = 1, 2, \cdots, N \tag{14}$$

For the TIC $\hat{y}$ is the estimated output from the identified model, and y is the measured output for each input i. The TIC has a value between 0 to 1, and a decent fit on a specific output should have a $\mathcal{T}_i < 0.3$.[24]

IV.D. Online Identification Procedure

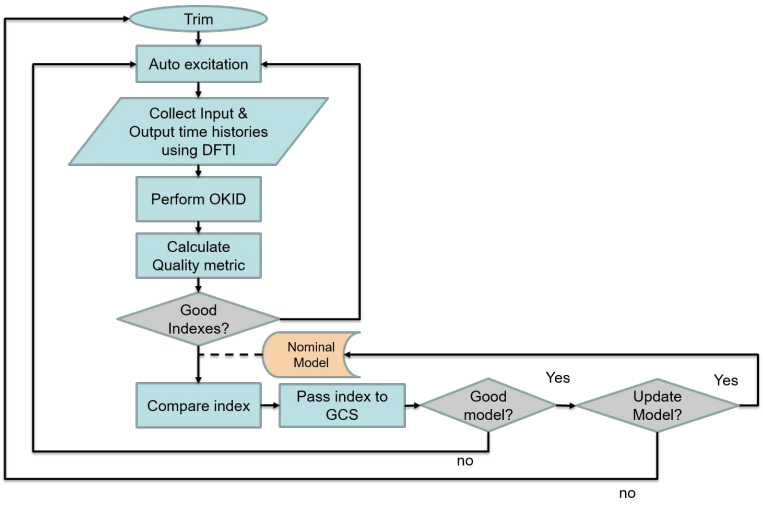

Figure 8: Online system identification update procedure

The human-in-the-loop model update procedure is initiated when the pilot flips the excitation switch on the transmitter, and ends when the GCS operator makes the decision for model update. Data is transfered from the aircraft to the GCS through XBees antennas, and communication between each subprocess follows the UDP/IP protocol. The update procedure is shown in Fig. 8.

Once initiated, DFTI stores an onboard data log of the full duration of the flight for offline data comparison. After the pilot manually trims the aircraft the GCS operator updates the stored excitation parameters on the vehicle through the Clark user interface shown in Fig. 6. Once the updated values are received the system reads and saves the trimmed effector deflections before excitation. The excitation is initiated only after the pilot flips the excitation switch on the transmitter to start the auto-excitation loop. Servo commands are then sent to the Pixhawk via Mavlink and the system identification interface starts up a log for each excitation. This log records the current input excitation signal, excitation states, and the identification results. The results are transferred to the GCS though Clark, showing the identification quality metrics introduced in Section IV.B along with additional information on the difference of the current identified model and the known nominal model. Finally, the GCS operator makes the model update decision. If the GCS operator decides to update the model, the information in the log for the current excitation will replace the log for the nominal model. Note that a nominal model can be preloaded but is not required for the update procedure. Additionally, the identification process can also support batch identification but with a higher computational time.

V. Flight Test Results

Flight tests were conducted at Texas A&M University RELLIS Campus in College Station, TX. All tests were during early morning to minimize the effect of winds aloft. Test inputs were applied only after the aircraft is trimmed. Figure 9 shows an example of the flight path of a lateral/directional excitation plotted in Google Earth.[25] The red section indicates the location where the pilot initiates the excitation. The blue and yellow sections show the first and second excitation respectively. Green areas are regions in which the pilot is in manual control.

Both piloted and automated excitations are injected during flight. Fig. 10 compares the input signal of a manually applied elevator sweep compared to a GCS specified and initiated automated sweep. The automated excitation has shown higher consistency in excitation amplitude as well as better precision in high frequency excitations. Note that both piloted and automated excitations are shown to be feasible for generating accurate flight models, but for online system identification the automated inputs are preferred.

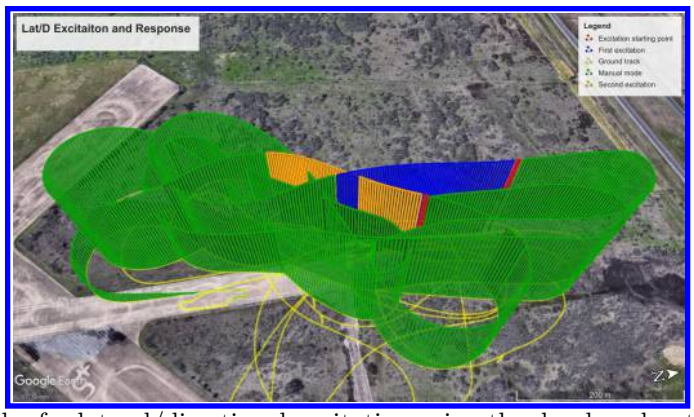

Figure 9: Flight path of a lateral/directional excitation using the developed auto-excitation method

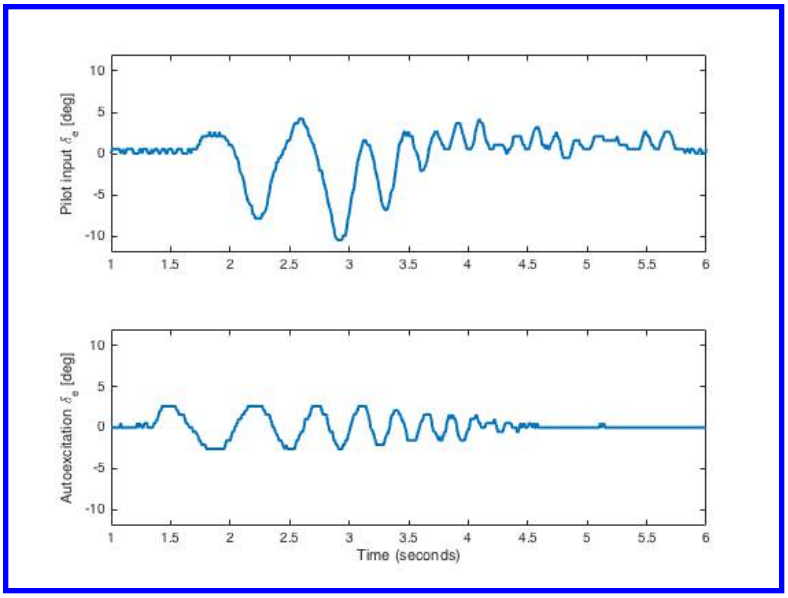

Figure 10: Comparison of human generated sine sweep versus auto-excitation method

The extent of variation of identified models and the inconsistency due to varying pilot inputs is shown in Fig. 11. It presents the progression of identified lat/d eigenvalues from a single flight under wind gusts not exceeding 5 mph. All of the data sets were acquired at similar trim conditions. The red marker represents the identified nominal model. The green marker indicates an identified model with a low TIC value, and the blue markers indicate results that have significant identification error, indicated by a TIC value above 0.5.

V.A. Manual Excitation Results

For manual inputs, data was collected and analyzed from 11 different flight days with 59 excitation maneuvers that combine both longitudinal and lateral/directional responses. The success rate in identifying a linear model with the right rank and modes was 24 percent on average. The poor consistency using manual inputs is demonstrated by the fact only 6 flight maneuvers yielded an identified model with a $\text{TIC}_{avg} < 0.3$ and fit the output response extremely well, which is a 10% rate of identifying a nominal model. Note that the number of time shifts in the Hankel matrices p was set to 10 for all identifications.

V.B. Automated Excitation Results

Longitudinal results from an automated sweep input applied to the elevator are shown in Fig. 12. The identified states are shown as dashed red while the actual flight data is solid blue. The input successfully excites both the phugoid and short period modes of the longitudinal model. Characteristics of the identified

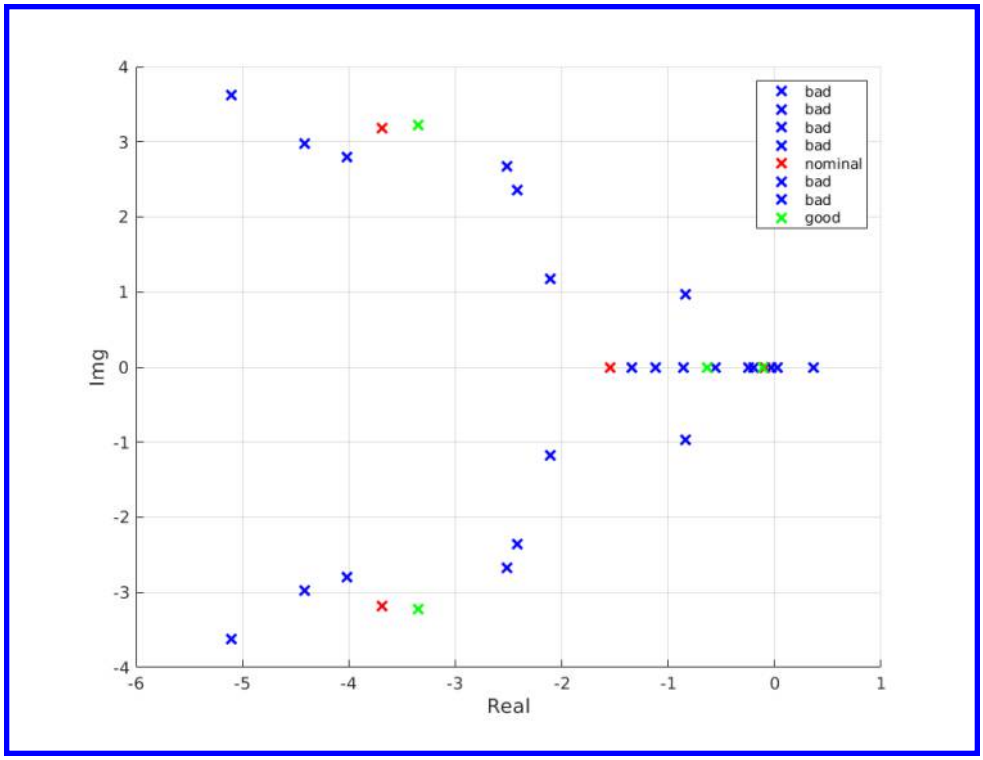

Figure 11: Accumulated identified eigenvalues of the multiple piloted and automated excitation results

model are shown in Table 2. Fig. 13 shows the results of a Lat/D maneuver set. The identified model has a low identification error between the estimated output and the measured output signal and the characteristics for the Lat/D model is shown in Table 3. It can be seen from Fig. 13 that around 1 second of the time history from the flight data showed data clipping due to the $\pm 20^{\circ}$ measuring limit imposed by the μADC. However, the identified results also exhibited that even with data clipping, the effect does not affect the identified results.

To quantify excitation input repeatability, two excitation data sets are compared. The two input sets were applied on different flight days but with the exact same configurations. Figure 14 shows a direct comparison of the measured input signals. The averaged TIC value of the two signals was 0.007, indicating the input sets are identical with negligible measurement noise difference. This validates input repeatability of the system.

Table 2: Super Cub longitudinal dynamic modes.

Mode	**Phugoid**	**Short Period**
Eigenvalue	$-0.13 \pm \mathrm{j}5.30$	$-6.36 \pm \mathrm{j}2.68$
Damping Ratio	0.23	0.92
Natural Freq. (rad/s)	0.09	1.01
MSV (%)	100.0	22.7
MCI (%)	54.2	100.0
MOI (%)	74.2	100.0

V.C. Online Full Lat/Lon System Identification

A full Lat/D and longitudinal multi-sine excitation combination is applied to acquire a full-order, fully coupled state-space linear model. With a goal of effectively exciting the rigid-body dynamic modes in a short time, several input excitation combinations were tested. Only the combination that is judged to be the most effective is presented here.

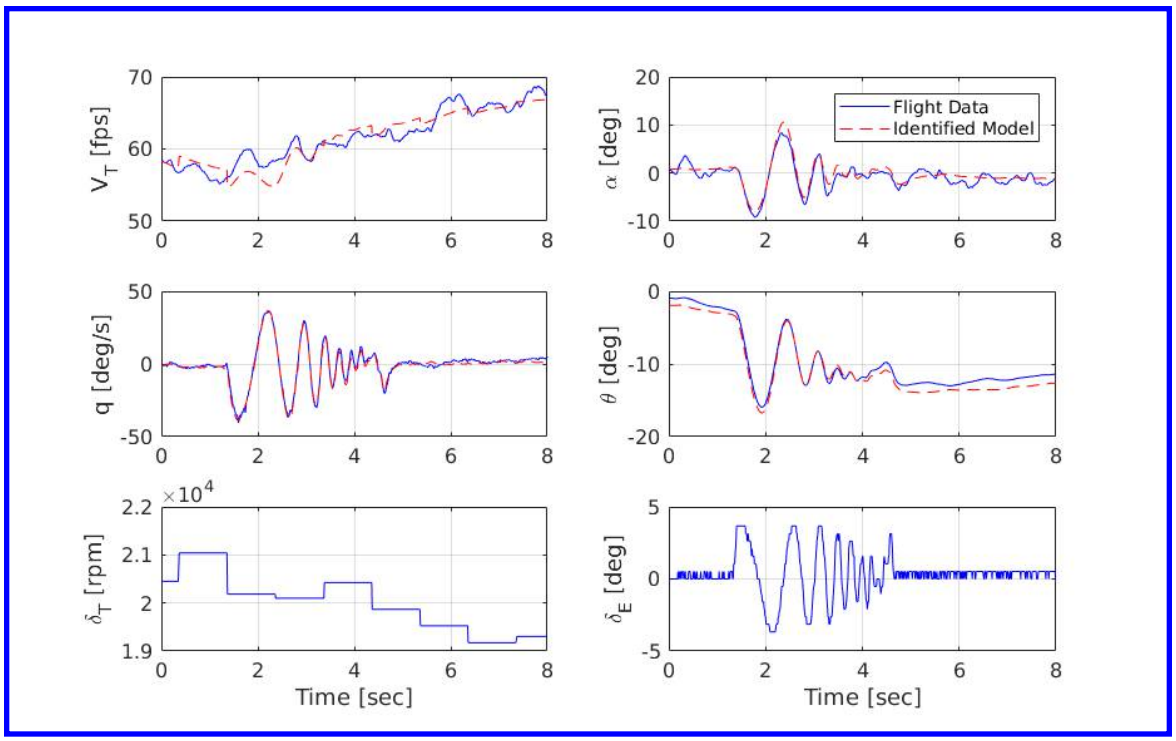

Figure 12: Identified longitudinal flight test results from automated inputs

Table 3: Super Cub lateral/directional dynamic modes.

Mode	Spiral	Roll	Dutch Roll
Eigenvalue	-0.038	-0.54	$-3.05 \pm \mathrm{j}3.67$
Damping Ratio	—	—	0.63
Natural Frequency (rad/s)	—	—	0.76
Time Constant (sec)	26.1	1.85	—
MSV (%)	100.0	41.4	31.9
MCI (%)	12.0	28.1	100
MOI (%)	96.7	100.0	93.1

Table 4 displays the input details for each multi-sine input for Eq. (11). The parameter A_k is the amplitude command in terms of PWM. All excitation inputs and analysis results shown in this subsection is directly collected via flight test with no additional processing. The input and output sets used are from the log files and the identification code is the exact same code as implemented onboard the vehicle. Application of

Table 4: Input parameters for multi-sine excitation.

Input	A_k **(PWM)**	**k**	RPF
δ_a	40	$3, 6, 9, 12$	1.51
δ_r	40	$5, 10, 15, 20$	1.21
δ_e	40	$7, 14, 21, 28$	1.52

a low frequency multi-sine wave input to the throttle appeared to be a reasonable approach, but experiments have shown that the time delay caused by the Electronic Speed Controller (ESC) response time restricts the excitation efficiency. Moreover, the asymmetric nonlinear change on ramping throttle input up and down results in a large RPF. Therefore, utilizing experience gained from manual input longitudinal system identification maneuvers, a step like input similar to the longitudinal input was applied to the throttle. Fig.

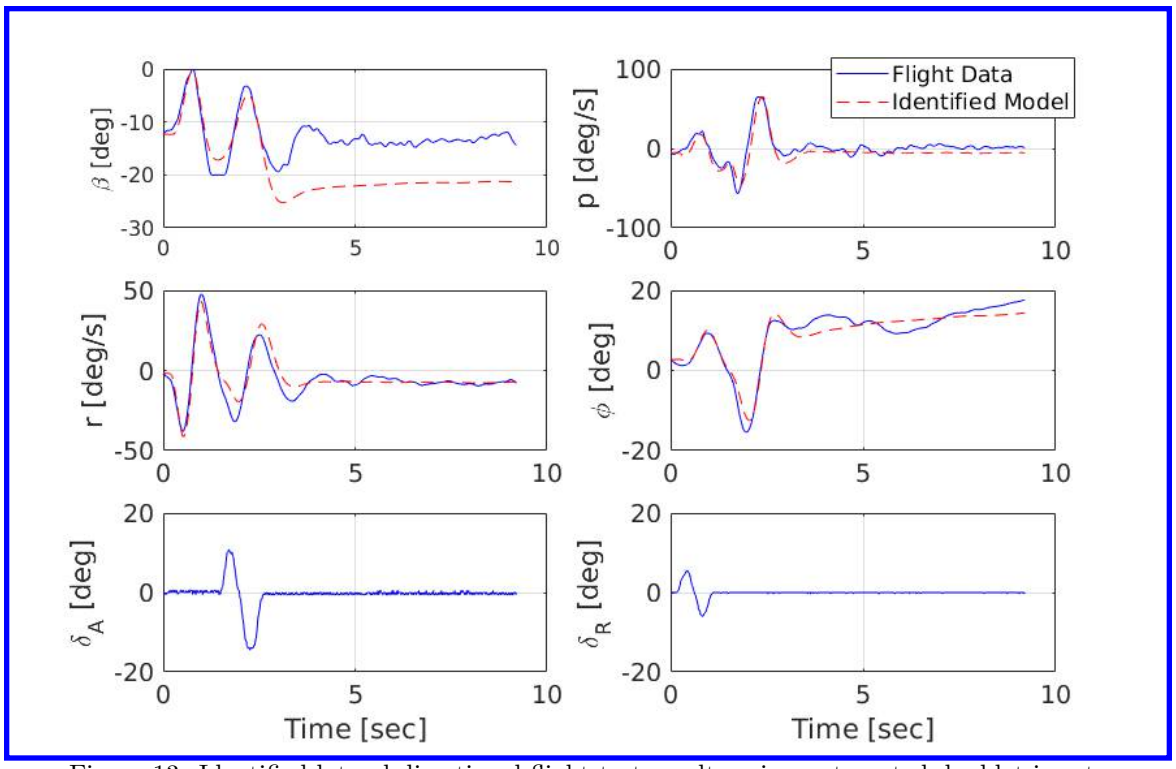

Figure 13: Identified lateral directional flight test results using automated doublet inputs

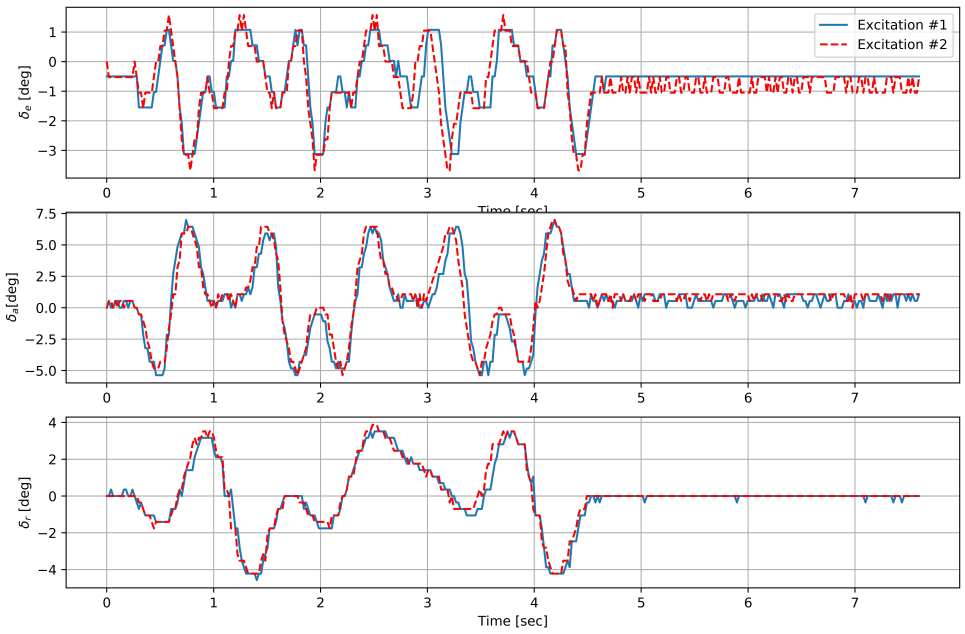

Figure 14: Comparison of two excitation signals with identifical settings

15 is the measured combined input data collected from DFTI. The identified and measured output results are shown in Figure 5 and produced an averaged TIC value of $T_{avg} = 0.21$, which indicates a very low error

between the estimated and measured state responses. The identified details are shown in Table 5.

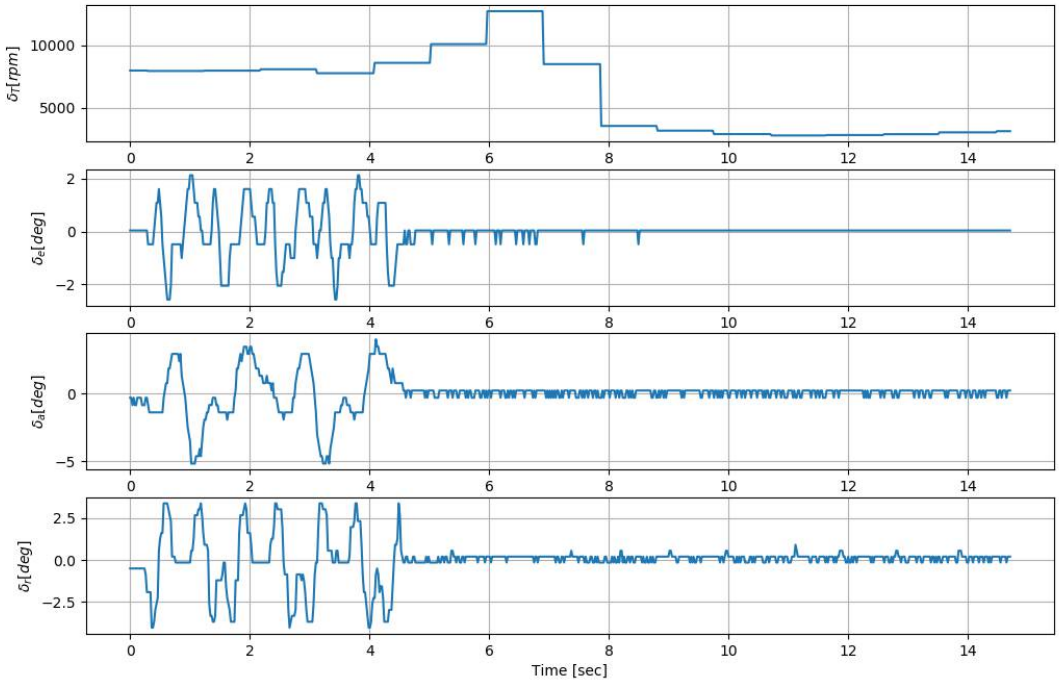

Figure 15: Combined multi-sine excitation applied on aileron, rudder, and elevator followed by a step-like throttle input sequence.

Table 5: Super Cub full Lat/Lon dynamic modes.

Mode	**Phugoid**	**Short Period**	**Spiral**	**Roll**	**Dutch Roll**
Eigenvalue	-0.18	-4.65	-0.84	-36.88	-1.17
	±j0.68	±j3.10			±3.88
Damping Ratio	0.26	0.83	—	—	0.29
Natural Freq. (rad/s)	0.11	0.89	—	—	0.64
Time Const. (sec)	—	—	1.19	0.03	—
MSV (%)	100.0	24.83	57.42	5.10	39.02
MCI (%)	79.49	70.54	100.0	21.75	41.78
MOI (%)	53.80	91.34	65.55	74.22	100.0

Automated input excitation has been shown to be superior to manually input excitation maneuvers in terms of both accuracy and repeatability. It is important for online near real-time system identification, and can also be utilized to perform different excitation sequences for more efficient excitations. In terms of the efficiency of identified results, excluding flights in the developmental stage the combined Lat/D and longitudinal excitation sequence recorded a 7 out of 21 success rate of identifying a system model with the correct modal composition, with a $\text{TIC}_{avg} < 0.3$. The success rate increased from 10% to 33% with an overall increase of 23 percent. Note that virtually all of the the identification failures were due to both poor manual trimming before excitation is initiated, and strong wind gusts that perturb the vehicle out of steady, level flight conditions.

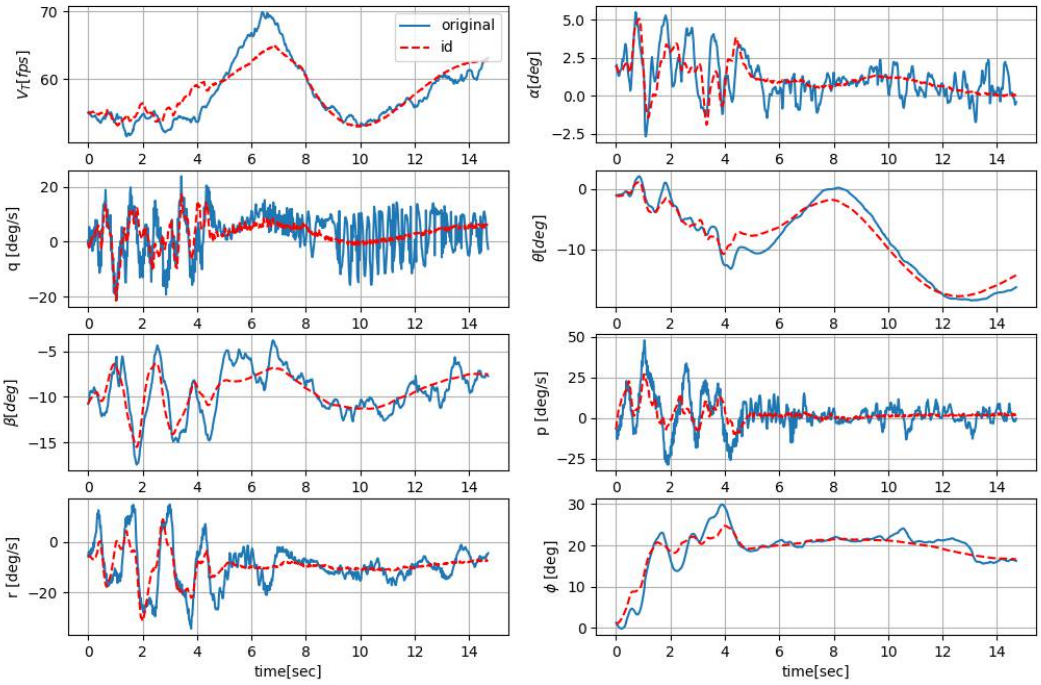

Figure 16: Full lateral/directional and longitudinal identification with the combined input excitation set.

VI. Conclusions

This paper presented a system capable of performing online near real-time system identification on Small Unmanned Air Systems using commercial off-the-shelf sensors and embedded computers, a custom data acquisition unit, and a custom communication system. Based on the results presented in the paper, the following conclusions are drawn:

1. An automated method of applying excitation inputs was shown to be capable of applying various excitations of the user's choice. An input combination was introduced for combined lateral/directional and longitudinal system identification on a Small Unmanned Air System. The full surface excitation was shown to be capable of exciting all of the vehicle rigid-body dynamic modes effectively in a single excitation sequence. In tests, the method yielded a repeatable and precise excitation with 99% of similarity and an identical power spectrum.

2. The human-in-the-loop system identification procedure using the custom system was shown to be capable of performing near real-time online identification using Commerical Off The Shelf products. The system produced identification results with a Theil Inequality Coefficient value smaller than 0.3 by 26%.

3. Observer Kalman Filter Identification yielded accurate identification results during flight tests and is a feasible candidate for online near real-time system identification on a SUAS.

Appendix

Below are identified longitudinal and lateral/directional linear time-invariant state-space models in stability axes for the Hangar-9 1/4 Scale PA-18 Super Cub. Angular states are in radians, angular rates in radians per second, velocity is in meters per second, and controls are in degrees. The aircraft weight is

20.5 lbf and the C.G. location is $0.27\bar{c}$. The trim flight condition is 200 feet altitude at $V_{T_1} = 58.92 ft/s$, $\alpha_1 = 0.43°$, $q_1 = -0.89\,°/\text{s}$, and $\theta_1 = -0.95°$.

$$\begin{Bmatrix} \dot{V}_T \\ \dot{\alpha} \\ \dot{q} \\ \dot{\theta} \end{Bmatrix} = \begin{bmatrix} -0.056 & 96.46 & -30.38 & -28.87 \\ -0.00018 & -3.42 & 1.777 & -0.2478 \\ 0.0061 & -7.731 & -8.646 & 0.8374 \\ -0.0003 & 0.05595 & 0.9849 & -0.1223 \end{bmatrix} \begin{Bmatrix} V_T \\ \alpha \\ q \\ \theta \end{Bmatrix} + \begin{bmatrix} -0.002194 & -70.2 \\ 0.0001651 & 2.126 \\ -0.000589 & -107.6 \\ 0.00003 & -0.4742 \end{bmatrix} \begin{Bmatrix} \delta_T \\ \delta_E \end{Bmatrix} \tag{VI.1}$$

The lateral/directional model is trimmed at $\beta_1 = -6.75°$, $p_1 = 2.2\,°/\text{s}$, $r_1 = -0.62\,°/\text{s}$, and $\phi_1 = -0.59°$, where a '1' subscript indicates a trim value.

$$\begin{Bmatrix} \dot{\beta} \\ \dot{p} \\ \dot{r} \\ \dot{\phi} \end{Bmatrix} = \begin{bmatrix} 0.113 & -0.1234 & -1.01 & -0.423 \\ 2.016 & -4.12 & -4.811 & -1.482 \\ 1.532 & 2.648 & -2.643 & -0.05058 \\ -0.03503 & 0.9893 & -0.1365 & -0.0373 \end{bmatrix} \begin{Bmatrix} \beta \\ p \\ r \\ \phi \end{Bmatrix} + \begin{bmatrix} 0.2866 & -0.1318 \\ -26.8 & -21.08 \\ 1.01 & -42.46 \\ -0.5747 & -0.05489 \end{bmatrix} \begin{Bmatrix} \delta_A \\ \delta_R \end{Bmatrix} \tag{VI.2}$$

For the full Lat/Lon model, Eq. (VI.3) is trimmed at $V_{T_1} = 53.2 ft/s$, $\alpha_1 = 6.9°$, $q_1 = -1.88\,°/\text{s}$, $\theta_1 = -2.3°$, $\beta_1 = -10.2°$, $p_1 = -9.1\,°/\text{s}$, $r_1 = 7.06\,°/\text{s}$, and $\phi_1 = -1.99°$.

$$\begin{Bmatrix} \dot{V}_T \\ \dot{\alpha} \\ \dot{q} \\ \dot{\theta} \\ \dot{\beta} \\ \dot{p} \\ \dot{r} \\ \dot{\phi} \end{Bmatrix} = \begin{bmatrix} -0.1024 & 53.82 & 1.628 & -17.27 & -12.32 & -8.126 & 7.578 & -4.461 \\ -0.001828 & -3.315 & 0.3846 & 0.2039 & -0.7053 & -0.2758 & 0.03408 & 0.07363 \\ -0.01013 & -11.45 & -8.006 & -0.8578 & -5.171 & -1.303 & 0.4311 & 1.716 \\ 7.135e-05 & 0.06239 & 0.7233 & 0.06777 & -0.1015 & 0.03443 & -0.1508 & 0.02052 \\ -0.0006755 & 0.1425 & 0.1199 & -0.05842 & -0.2276 & 0.1202 & -1.196 & -0.4859 \\ 0.02233 & 18.57 & -2.621 & -1.03 & 7.146 & -6.787 & -1.459 & -0.6098 \\ 0.0319 & 2.792 & -6.899 & 0.04692 & 9.054 & 1.324 & -3.227 & -0.5634 \\ -0.002979 & -1.261 & -0.3331 & -0.09967 & -0.4313 & 0.715 & -0.3139 & -0.686 \end{bmatrix} \begin{Bmatrix} V_T \\ \alpha \\ q \\ \theta \\ \beta \\ p \\ r \\ \phi \end{Bmatrix} + \begin{bmatrix} 0.0004221 & 131.4 & -70.86 & 90.43 \\ 0.000003 & -9.345 & 1.082 & 0.5909 \\ 0.0001414 & -85.4 & -1.014 & 8.59 \\ 0.0000016 & -4.301 & -0.0724 & 0.1515 \\ 0.0000043 & 2.283 & 0.0291 & -1.359 \\ 0.000018 & -2.751 & -31.31 & 10.12 \\ 0.000029 & -40.41 & -2.808 & -47.15 \\ 0.000005 & -2.634 & -3.098 & -1.568 \end{bmatrix} \begin{Bmatrix} \delta_T \\ \delta_E \\ \delta_A \\ \delta_R \end{Bmatrix} \tag{VI.3}$$

References

[1]Bushnell, D. M., "Scaling: wind tunnel to flight," *The Annual Review of Fluid Dynamics*, Vol. 38, 2006, pp. 111–121.

[2]DeBusk, W., Johnson, E., and Chowdhary, G., "Real-time system identification of a small multi-engine aircraft," *AIAA Atmospheric Flight Mechanics Conference*, 2009, p. 5935.

[3]Jameson, P.-D. and Cooke, A., "Developing real-time system identification for UAVs," *Control (CONTROL), 2012 UKACC International Conference on*, IEEE, 2012, pp. 958–963.

[4]Ahmed-Zaid, F., Ioannou, P., and Polycarpou, "Identification and control of aircraft dynamics using radial basis function networks," *Control Applications, 1993., Second IEEE Conference on*, 1993.

[5]Morelli, E. A., "Real-Time Global Nonlinear Aerodynamic Modeling for Learn-To-Fly," *AIAA Atmospheric Flight Mechanics Conference*, 2016, p. 2010.

[6]Klein, V. and Morelli, E. A., *Aircraft System Identification: Theory and Practice*, American Institute of Aeronautics and Astronautics Reston, Va, USA, 2006.
[7]Morelli, E. A., Cunningham, K., and Hill, M. A., "Global Aerodynamic Modeling for Stall/Upset Recovery Training Using Efficient Piloted Flight Test Techniques," *AIAA Modeling and Simulation Technologies (MST) Conference*, 2013, p. 4976.
[8]Valasek, J. and Chen, W., "Observer/Kalman filter identification for online system identification of aircraft," *Journal of Guidance, Control, and Dynamics*, Vol. 26, 2003, pp. 347–353.
[9]Arthurs, F., Valasek, J., and Zeigler, M. D., "Precision Onboard Small Sensor System for Unmanned Air Vehicle Testing and Control," *Proceedings of the AIAA Guidance, Navigation, and Control Conference*, San Diego, CA, 2016.
[10]Lu, H.-H., Harris, J., Goecks, V., and Valasek, J., "Flight Test Instrumentation for Small UAS System Identification," *Unmanned Aircraft Systems (ICUAS), 2017 International Conference on*, IEEE, 2017.
[11]Harris, J., Goecks, V. G., Lu, H.-H., and Valasek, J., "VSCL Developmental Flight Test Instrumentation," May 2017.
[12]Rogers, Cameron, N. C. and Valasek, J., "Heterogeneous Multi-Vehicle Modular Control Framework With Payload Integration," *Unmanned Aircraft Systems (ICUAS), 2017 International Conference on*, IEEE, 2017.
[13]Iliff, K. W., "Parameter estimation for flight vehicles," *Journal of Guidance, Control, and Dynamics*, Vol. 12, No. 5, 1989, pp. 609–622.
[14]Juang, J.-N., *Applied System Identification*, Prentice Hall, Upper Saddle River, NJ, 1994.
[15]Woodbury, T. D., Valasek, J., and Arthurs, F., "Flight test results of Observer/Kalman Filter Identification of the Pegasus unmanned vehicle," *AIAA Atmospheric Flight Mechanics Conference*, 2015, p. 1481.
[16]Jared A. Grauer, E. A. M. and Murri, D. G., "Flight Test Techniques for Quantifying Pitch Rate and Angle of Attack Rate Dependencies," *AIAA Atmospheric Flight Mechanics Conference*, 2017.
[17]Maine, R. E. and Iliff, K. W., "Maximum likelihood estimation of translational acceleration derivatives from flight data," *Journal of Aircraft*, Vol. 16, No. 10, 1979, pp. 674–679.
[18]Schroeder, M., "Synthesis of low-peak-factor signals and binary sequences with low autocorrelation (corresp.)," *IEEE Transactions on Information Theory*, Vol. 16, No. 1, 1970, pp. 85–89.
[19]Morelli, E. A., "Multiple input design for real-time parameter estimation in the frequency domain," *IFAC Proceedings Volumes*, Vol. 36, No. 16, 2003, pp. 639–644.
[20]Meier, L., Honegger, D., and Pollefeys, M., "PX4: A Node-Based Multithreaded Open Source Robotics Framework for Deeply Embedded Platforms," *Robotics and Automation (ICRA), 2015 IEEE International Conference on*, May 2015.
[21]"Pixhawk 2 overview," 2017, Accessed 04 December 2017.
[22]Longman, R., Bergmann, M., and Juang, J.-N., "Variance and bias confidence criteria for ERA modal parameter identification," *Astrodynamics Conference*, 1988, p. 4312.
[23]Pappa, R. S., Elliott, K. B., and Schenk, A., "Consistent-mode indicator for the eigensystem realization algorithm," *Journal of Guidance, Control, and Dynamics*, Vol. 16, No. 5, 1993, pp. 852–858.
[24]Jategaonkar, R., *Flight vehicle system identification: a time domain methodology*, Vol. 216, AIAA, Reston, VA, USA, 2006.
[25]"Google Earth Pro," 2017, Accessed 04 December 2017.